



# An afterburner-powered methane/steam reformer for a solid oxide fuel cells application

Marcin Mozdierz<sup>1</sup> · Maciej Chalusiak<sup>1</sup> · Shinji Kimijima<sup>2</sup> · Janusz S. Szmyd<sup>1</sup> · Grzegorz Brus<sup>1</sup>

Received: 10 April 2017 / Accepted: 26 March 2018 / Published online: 5 April 2018  
© The Author(s) 2018

## Abstract

Solid oxide fuel cell (SOFC) systems can be fueled by natural gas when the reforming reaction is conducted in a stack. Due to its maturity and safety, indirect internal reforming is usually used. A strong endothermic methane/steam reforming process needs a large amount of heat, and it is convenient to provide thermal energy by burning the remainders of fuel from a cell. In this work, the mathematical model of afterburner-powered methane/steam reformer is proposed. To analyze the effect of a fuel composition on SOFC performance, the zero-dimensional model of a fuel cell connected with a reformer is formulated. It is shown that the highest efficiency of a solid oxide fuel cell is achieved when the steam-to-methane ratio at the reforming reactor inlet is high.

## List of symbols

$a, b$	reaction orders, (-)	$\Delta h$	change of enthalpy associated with reaction, (J mol <sup>-1</sup> )
$A_{\text{cell}}$	cell active area, (m <sup>2</sup> )	$\Delta h^0$	change of enthalpy associated with reaction in standard reference state, (J mol <sup>-1</sup> )
$A_{\text{msr}}$	Arrhenius constant, (mol s <sup>-1</sup> kg <sup>-1</sup> Pa <sup>-(a+b)</sup> )	$i$	electric load, (A m <sup>-2</sup> )
$c, e$	Tafel equation coefficients, (V)	$i_0$	exchange current density, (A m <sup>-2</sup> )
$C_p$	constant pressure specific heat, (J mol <sup>-1</sup> K <sup>-1</sup> )	$i_{\text{lim}}$	limiting current density, (A m <sup>-2</sup> )
$d$	electrode thickness, (m)	$K_p$	permeability, (m <sup>2</sup> )
$\bar{D}$	averaged diffusion coefficient, (m <sup>2</sup> s <sup>-1</sup> )	$M_i$	molar mass of species $i$ , (kg mol <sup>-1</sup> )
$D_j$	diffusion coefficient of species $j$ , (m <sup>2</sup> s <sup>-1</sup> )	$n$	number of transferred electrons, (-)
$E_a$	activation energy, (J mol <sup>-1</sup> )	$\dot{n}_i^{\text{inlet}}$	inlet molar flow of species $i$ , (mol s <sup>-1</sup> )
$E_{\text{cell}}$	fuel cell potential, (V)	$OCV$	open circuit voltage, (V)
$E_{\text{rev}}$	fuel cell reversible potential, (V)	$p_i$	partial pressure of species $i$ , (Pa)
$E_{\text{in}}$	thermoneutral fuel cell potential, (V)	$P$	absolute pressure, (Pa)
$f$	inertia coefficient, (-)	$P_{\text{cell}}$	fuel cell power (W)
$F$	Faraday constant, $F = 96485.3329 \text{ C mol}^{-1}$	$Q$	heat of reaction, (W)
		$R$	reaction rate (mol s <sup>-1</sup> m <sup>-3</sup> ),
		$\bar{R}$	universal gas constant, $R = 8.314472 \text{ J mol}^{-1} \text{ K}^{-1}$
		$R_{\text{cell}}$	fuel cell electric resistance, ( $\Omega \text{ m}^2$ )
		$SC$	steam-to-methane ratio, (-)
		$T$	temperature, (K)
		$U$	velocity, (m s <sup>-1</sup> )
		$U_f$	utilization factor, (-)
		$w_{\text{cat}}$	catalyst weight density, (kg m <sup>-3</sup> )
		$ycr$	carbon monoxide conversion rate, (-)
		$Y_j$	molar fraction of species $j$ , (-)

✉ Marcin Mozdierz  
marcinm@agh.edu.pl

<sup>1</sup> Department of Fundamental Research in Energy Engineering, AGH University of Science and Technology, 30 Mickiewiczza ave., Krakow, Poland

<sup>2</sup> Shibaura Institute of Technology, College of Systems Engineering and Science, Department of Machinery and Control Systems, 307 Fukasaku, Minuma-ku, Saitama, Japan

## Greek

$\varepsilon$	efficiency, (-)
$\eta$	overpotential, (V)
$\varphi$	porosity, (-)
$\lambda$	thermal conductivity, ( $\text{W m}^{-1} \text{K}^{-1}$ )
$\mu$	dynamic viscosity, (Pa s)
$\rho$	density, ( $\text{kg m}^{-3}$ )
$\tau$	tortuosity factor, (-)

## Subscripts and superscripts

act	activation overpotential
cell	solid oxide fuel cell
conc	concentration overpotential
eff	effective value
in	inlet
max	maximal
mix,H	mixture of gases inside the heating channel
mix,R	mixture of gases inside the reformer
msr	methane/steam reforming reaction
N	Nernst overpotential
O	ohmic overpotential
s	solid particles
w	solid wall
wgs	water-gas shift reaction

## 1 Introduction

The methane/steam reforming is the most important hydrogen and syngas production process for industrial scales [27]. One of the possible applications of a methane/steam reforming reactor is to use it as a fuel processor for high-temperature fuel cells, especially for solid oxide fuel cells (SOFCs), because high-temperature fuel cells can utilize hydrogen as well as carbon monoxide in the electrochemical reactions.

Due to its endothermic nature, the methane/steam reforming process needs a large amount of heat to produce syngas. In conventional reforming facilities, a part of the provided methane is partially burned to heat up the reactor, which leads to significant fuel losses. There are several existing methods to bypass this problem. For example, it is possible to use heat produced in a high-temperature nuclear reactor [14, 28] or to conduct a so-called direct internal reforming process, i.e., the reforming process occurs directly on the SOFC anode [9], which is the exquisite catalyst for the methane/steam reforming reaction [22]. The latter solution allows utilizing heat produced in SOFC electrochemical reactions and assist in the proper design of fuel cell thermal management [6]. However, this procedure does not yet reach commercial potential due to the occurrence of thermal stresses inside fuel cell and carbon formation phenomena.

In solid oxide fuel cells the fuel starvation phenomena may occur, which means that fuel is consumed completely inside the cell. This leads to the oxidation of the nickel anode and consequently to cell destruction [4]. Due to this issue, some amount of provided fuel does not take part in the electrochemical reactions (usually 20–30% of the provided fuel) [1]. Unused fuel can be utilized in the afterburner, for example, to produce heat for a central heating system. However, in a combined reformer-SOFC system, it is possible to exploit combustion products, which stand out for high sensible thermal enthalpy, in the in-stack heat exchanger-type methane/steam reformer [14]. This solution is a type of indirect internal reforming [2], which prevents problems related to direct internal reforming. One of the possible configurations of the proposed system is presented on Fig. 1.

Several research groups focus on coupling methane/steam reforming with fuel cells. Nishino et al. [19] prepared the model of an in-cell methane/steam reformer and discussed methods of smoothing the temperature field inside the system. It was shown that the proper design of a methane/steam reformer helps in the cooling of the cell. The model was later used by Nishino and Szymd [18] to analyze a SOFC unit combined with a steam reformer of biogas. Brus [3] experimentally investigated reforming kinetics on the Ni/SDC catalyst and successfully implemented it into the computational fluid dynamics (CFD) model of the methane/steam reformer which can be used in combination with high-temperature fuel cells. Sciazko with coworkers [23] analyzed the kinetics of methane/steam reforming reaction using the generalized least squares method for SOFC modeling. Mozdierz et al. [15] conducted parametric studies on the methane/steam reforming reaction and concluded that the adaptation of heating zones and localized catalyst density can significantly help in process control.

Power/efficiency analysis was also investigated in the past to analyze the impact of working conditions on SOFC performance. The quasi-2D model built by the Suzuki group [24] was used to determine the efficiency of the fuel cell alone and the solid oxide fuel cell-micro gas turbine hybrid power system (SOFC-MGT). This model was later expanded to include the effect of biogas on system performance [25] and to answer the following question: how does the SOFC-MGT system behave under part-load conditions [10]. The system analysis in the above-mentioned works is, among others, based on efficiency and power analysis. Zhu and Kee [29] presented a model of SOFC efficiency and fuel utilization. They showed that maximal possible efficiency is independent of actual system design, i.e. membrane/electrode assembly characteristics or polarization losses. However, power density depends on an overvoltage, thus the proper design of the cell size and

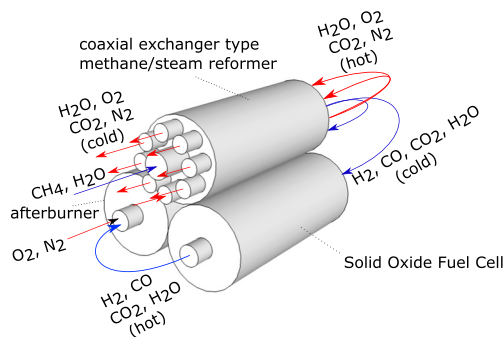


**Fig. 1** Possible configuration of the SOFC-afterburner-reformer system

architecture is essential to minimize losses and increase the power density.

Ni [16] analyzed hydrogen production in a compact reformer for fuel cell applications. He assumed that the constant heat flux is conducted from the combustion duct to the reforming duct, however, the heat flux was treated as the boundary condition. His parametric studies show possibility for optimization of reforming reactor and point that proper combustion control may lead to higher reaction rates. Powell et al. [21] present results of the experimental investigation of an indirect reforming system, where anode gases are recirculated and provide energy for the reforming reaction. In addition to works which analyze the hydrocarbons reforming in indirect process within the SOFC, the present paper shows the CFD model of a heat exchanger-type methane/steam reforming device, which uses gases from the SOFC afterburner as a source of energy to activate the reforming reaction. The output from this model is a temperature field inside the system and molar fraction distributions in the reformer. The species molar fractions at the reformer outlet are input data for the zero-dimensional solid oxide fuel cell model, which can predict cell power and efficiency (please note that this is the efficiency of SOFC only, not the efficiency of the whole system).

## 2 Mathematical model

The mathematical model is divided into two parts: the reformer model and the SOFC model. The heat exchanger-type reformer consists of two concentric tubes, where the inner tube is filled with a catalyst, nickel and yttria-stabilized zirconia metal foam (Ni/YSZ 40:60% vol.). Through the outer tube there is a flow of a mixture of  $\text{CO}_2$  and  $\text{H}_2\text{O}$ , leftover fuel cell combustion products, which destination is to provide heat for the endothermic methane reforming reaction. A schematic sketch of the hydrogen production system is presented in Fig. 2. The system works

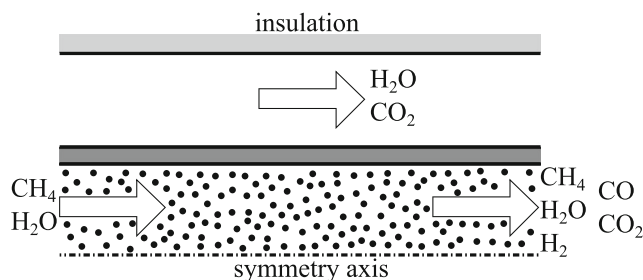


**Fig. 2** Schematic view on the heat exchanger-type methane steam reformer

in a parallel-flow set-up because for heat exchanger-type reforming reactors it is a preferable configuration [14] and it is axisymmetric, as shown in Fig. 2.

### 2.1 The methane/steam reforming model

The methane/steam reforming process can be reduced to two dominant reactions: the methane/steam reforming reaction, Eq. 1, and the water-gas shift reaction, Eq. 2.



The standard enthalpy of the methane/steam reforming reaction is  $\Delta h_{\text{msr}}^0 = 206.1 \text{ kJ mol}^{-1}$ , thus the reaction is strongly endothermic. Reaction (1) is slow, therefore the rate of reaction is necessary. The reaction rate can be formulated as follows:

$$R_{\text{msr}} = w_{\text{cat}} A_{\text{msr}} \exp\left(-\frac{E_a}{RT}\right) p_{\text{CH}_4}^a p_{\text{H}_2\text{O}}^b, \quad (3)$$

where  $w_{\text{cat}}$  [ $\text{kg m}^{-3}$ ] stands for the catalyst weight density and  $p_i$  [Pa] is the partial pressure of species  $i$ . Arrhenius constant  $A_{\text{msr}} = 0.09617 \text{ mol s}^{-1} \text{ kg}^{-1} \text{ Pa}^{-0.61}$ , activation energy  $E_a = 43920 \text{ J mol}^{-1}$  and reaction orders with respect to the methane  $a = 0.39$  and with respect to the steam  $b = 0.22$ , which appear in Eq. 3 has been obtained experimentally, according to [13].

The standard enthalpy of water-gas shift reaction Eq. 2 is  $\Delta h_{\text{wgs}}^0 = -41.15 \text{ kJ mol}^{-1}$ , which indicates that the reaction is exothermic, however, in comparison with the enthalpy of the reaction (1), the whole process is endothermic. It is assumed that the water-gas shift reaction is in equilibrium in the temperature of the reforming process, thus the reaction rate can be derived from equilibrium equation and partial pressures of species [15] as follows:

$$R_{\text{wgs}} = R_{\text{msr}} y_{\text{cr}}, \quad (4)$$

where  $y_{\text{cr}}$  [–] is the carbon monoxide conversion rate during the water-gas shift reaction.

**Table 1** Mass sources/sinks

Species	Mass source/sink
H <sub>2</sub>	$3R_{\text{msr}}M_{\text{H}_2} + R_{\text{wgs}}M_{\text{H}_2}$
CO	$R_{\text{msr}}M_{\text{CO}} - R_{\text{wgs}}M_{\text{CO}}$
CO <sub>2</sub>	$R_{\text{wgs}}M_{\text{CO}_2}$
CH <sub>4</sub>	$-R_{\text{msr}}M_{\text{CH}_4}$
H <sub>2</sub> O	$-R_{\text{msr}}M_{\text{H}_2\text{O}} - R_{\text{wgs}}M_{\text{H}_2\text{O}}$

Based on the reaction rates, the thermodynamic heat generation can be calculated:

$$Q_{\text{msr}} = -R_{\text{msr}}\Delta h_{\text{msr}}^0, \quad (5)$$

$$Q_{\text{wgs}} = -R_{\text{wgs}}\Delta h_{\text{wgs}}^0. \quad (6)$$

The reaction rates together with the stoichiometry of the chemical reactions, Eqs. 1 and 2, contribute to mass sources and sinks during the reforming process (shown in Table 1).

## 2.2 Model of heat and mass transfer inside the reformer

The computational domain, marked in Fig. 2, has been divided into three parts with different governing equations adapted: porous reformer catalyst, the separating wall and the heating tube. As stated above, the analyzed hydrogen producing device is axisymmetric. Thus, equations can be formulated in the two-dimensional cylindrical coordinate system. On the reformer inlet, there is the only mixture of methane and steam. All gases in the system are treated as ideal gases and the laminar flow assumption is undertaken. For the reacting gas mixture flow inside the methane/steam reforming reactor, the governing equations for the flow inside the porous media are applied.

The continuity equation within the reformer is written as:

$$\frac{\partial(\rho_{\text{mix,R}}U_x)}{\partial x} + \frac{1}{r}\frac{\partial(r\rho_{\text{mix,R}}U_r)}{\partial r} = 0, \quad (7)$$

where  $U_x$  and  $U_r$  [m s<sup>-1</sup>] stand for gas mixture velocity in  $x$  and  $r$  direction respectively, and  $\rho_{\text{mix,R}}$  [kg m<sup>-3</sup>] is the gas mixture density.

The velocity of the fluid flow within the porous material is calculated using the momentum transport equations, which have been derived from Forchheimer's extension of Darcy's law [17, 19].

$$\begin{aligned} & \frac{\rho_{\text{mix,R}}}{\varphi^2} \left( U_x \frac{\partial U_x}{\partial x} + U_r \frac{\partial U_x}{\partial r} \right) = -\frac{\partial P}{\partial x} \\ & + \frac{1}{\varphi} \left[ \frac{\partial}{\partial x} \left( \mu_{\text{mix,R}} \frac{\partial U_x}{\partial x} \right) + \frac{1}{r} \frac{\partial}{\partial r} \left( r \mu_{\text{mix,R}} \frac{\partial U_x}{\partial r} \right) \right] \\ & - \frac{\mu_{\text{mix,R}}}{K_p} U_x - \frac{\rho_{\text{mix,R}} f}{\sqrt{K_p}} U_x \sqrt{U_x^2 + U_r^2}, \end{aligned} \quad (8)$$

$$\begin{aligned} & \frac{\rho_{\text{mix,R}}}{\varphi^2} \left( U_x \frac{\partial U_r}{\partial x} + U_r \frac{\partial U_r}{\partial r} \right) = -\frac{\partial P}{\partial r} \\ & + \frac{1}{\varphi} \left[ \frac{\partial}{\partial x} \left( \mu_{\text{mix,R}} \frac{\partial U_r}{\partial x} \right) + \frac{1}{r} \frac{\partial}{\partial r} \left( r \mu_{\text{mix,R}} \frac{\partial U_r}{\partial r} \right) \right] \\ & - \frac{\mu_{\text{mix,R}}}{\varphi r^2} U_r - \frac{\mu_{\text{mix,R}}}{K_p} U_r - \frac{\rho_{\text{mix,R}} f}{\sqrt{K_p}} U_r \sqrt{U_x^2 + U_r^2}, \end{aligned} \quad (9)$$

where  $\varphi=0.9$  stands for the porosity and  $K = 1.0 \cdot 10^{-7}$  m<sup>2</sup> is the permeability of the porous catalyst,  $f = 0.088$  is the inertia coefficient, according to Nishino et al. [19] and  $\mu_{\text{mix}}$  [Pa s] is the mixture dynamic viscosity. Please note that the term  $\sqrt{U_x^2 + U_r^2}$  is the length of the local velocity vector.

Energy conservation is formulated using the Local Thermal Equilibrium model, which assumes that gases are in thermal equilibrium with the solid parts within porous domain. The physical values (e.g. temperature) are averaged locally between a solid and a fluid phase for a representative control volume [17].

$$\begin{aligned} & \rho_{\text{mix,R}} C_{p,\text{mix,R}} \left( U_x \frac{\partial T}{\partial x} + U_r \frac{\partial T}{\partial r} \right) \\ & = \frac{\partial}{\partial x} \left( \lambda_{\text{eff}} \frac{\partial T}{\partial x} \right) + \frac{1}{r} \frac{\partial}{\partial r} \left( r \lambda_{\text{eff}} \frac{\partial T}{\partial r} \right) + Q_s, \end{aligned} \quad (10)$$

where  $T$  [K] is the average temperature of both gas and solid phase and  $C_{p,\text{mix,R}}$  [J kg<sup>-1</sup> K<sup>-1</sup>] is the constant-pressure specific heat capacity of the gas mixture, calculated with the mixing laws [20].  $\lambda_{\text{eff}}$  [W m<sup>-1</sup> K<sup>-1</sup>] is the effective thermal conductivity of both the gas mixture and solid phase and it is calculated with formula  $\lambda_{\text{eff}} = \varphi \lambda_{\text{mix,R}} + (1 - \varphi) \lambda_s$ , where subscript 'mix,R' stands for mixture thermal conductivity, calculated using the Wassiljewa equation [20], and 's' stands for solid phase thermal conductivity ( $\lambda_s = 20$  [W m<sup>-1</sup> K<sup>-1</sup>] [19]).

Species conservation is based on the Fickian diffusion model and it is formulated on a molar fraction basis:

$$\begin{aligned} & \rho_{\text{mix,R}} \left( U_x \frac{\partial Y_j}{\partial x} + U_r \frac{\partial Y_j}{\partial r} \right) = \frac{\partial}{\partial x} \left( \rho_{\text{mix,R}} D_{j,\text{eff}} \frac{\partial Y_j}{\partial x} \right) \\ & + \frac{1}{r} \frac{\partial}{\partial r} \left( r \rho_{\text{mix,R}} D_{j,\text{eff}} \frac{\partial Y_j}{\partial r} \right) + S_j, \end{aligned} \quad (11)$$

where  $Y_j$  [-] is the molar fraction of species  $j$ .  $D_{j,\text{eff}}$  [m<sup>2</sup> s<sup>-1</sup>] is the effective diffusion coefficient of the gas mixture calculated with the correlation  $D_{j,\text{eff}} = (1 - \sqrt{1 - \varphi}) D_j$ , where diffusion of species  $j$  in a mixture of gases  $D_j$  is calculated with the Fuller et al. method and Blanc's law [20].

The source terms in the energy equation Eq. 10 and mass equation Eq. 11 are the results of methane/steam reforming and water-gas shift reactions, as described in Section 2.1.

Since the flow of heating gases (H<sub>2</sub>O and CO<sub>2</sub>) is non-reacting, the governing equations may be formulated as follows. The subscript ‘mix,H’ indicates that thermophysical properties for a mixture of H<sub>2</sub>O and CO<sub>2</sub> are used [26].

Continuity equation:

$$\frac{\partial (\rho_{\text{mix,H}} U_x)}{\partial x} + \frac{1}{r} \frac{\partial (r \rho_{\text{mix,H}} U_r)}{\partial r} = 0. \tag{12}$$

The momentum equations are the Navier-Stokes equations for the flow in the cylindrical coordinate system, since the heating channel contains no porous material [19].

$$\rho_{\text{mix,H}} \left( U_x \frac{\partial U_x}{\partial x} + U_r \frac{\partial U_x}{\partial r} \right) = - \frac{\partial P}{\partial x} + \frac{\partial}{\partial x} \left( \mu_{\text{mix,H}} \frac{\partial U_x}{\partial x} \right) + \frac{1}{r} \frac{\partial}{\partial r} \left( r \mu_{\text{mix,H}} \frac{\partial U_x}{\partial r} \right), \tag{13}$$

$$\rho_{\text{mix,H}} \left( U_x \frac{\partial U_r}{\partial x} + U_r \frac{\partial U_r}{\partial r} \right) = - \frac{\partial P}{\partial r} + \frac{\partial}{\partial x} \left( \mu_{\text{mix,H}} \frac{\partial U_r}{\partial x} \right) + \frac{1}{r} \frac{\partial}{\partial r} \left( r \mu_{\text{mix,H}} \frac{\partial U_r}{\partial r} \right) - \frac{\mu_{\text{mix,H}}}{r^2} U_r. \tag{14}$$

In the energy equation  $T$  [K] stands for the gas temperature (not locally averaged, since the heating tube is not filled with porous material).

$$\rho_{\text{mix,H}} C_{p,\text{mix,H}} \left( U_x \frac{\partial T}{\partial x} + U_r \frac{\partial T}{\partial r} \right) = \frac{\partial}{\partial x} \left( \lambda_{\text{mix,H}} \frac{\partial T}{\partial x} \right) + \frac{1}{r} \frac{\partial}{\partial r} \left( r \lambda_{\text{mix,H}} \frac{\partial T}{\partial r} \right). \tag{15}$$

In the solid wall, separating the reformer and heating channel, the only transport phenomena is heat conduction:

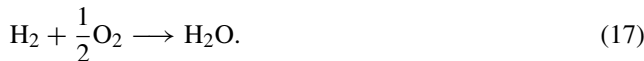
$$0 = \frac{\partial}{\partial x} \left( \lambda_w \frac{\partial T}{\partial x} \right) + \frac{1}{r} \frac{\partial}{\partial r} \left( r \lambda_w \frac{\partial T}{\partial r} \right). \tag{16}$$

The wall is made from ceramic material and  $\lambda_w = 1.1 \text{ W m}^{-1} \text{ K}^{-1}$  is the wall thermal conductivity [19].

The boundary conditions are presented in Fig. 3. The system pressure equals the atmospheric pressure. The temperature field for the subdomains was conjugated with the assumption of equality of the heat flux and the temperature at the boundaries. The partial differential equations have been discretized with the Finite Volume Method and the resulting systems of algebraic equations have been solved iteratively with the Gauss-Seidel method. To solve the governing equations, in-house C++ code has been built [15].

### 2.3 Solid oxide fuel cell model

A methane/steam reformer can be used as a fuel processor for a solid oxide fuel cell. To investigate the impact of inlet fuel mixture composition on SOFC performance, the zero-dimensional thermodynamic model of a single fuel cell was formulated. The model can predict cell’s power and efficiency using the working temperature, the composition of fuel at a cell’s inlet and the electric load as input data. In this study, it is assumed that the only reaction, which occurs in the solid oxide fuel cell, is the hydrogen oxidation reaction, whereas methane and carbon monoxide take part in the direct reforming on the anode.



From the reaction Eq. 17 it is clear that the number of exchanged electrons is  $n = 2 \text{ mol}_e^- \text{ mol}_{\text{H}_2}^{-1}$ .

Actual cell potential may be expressed as the difference between reversible cell potential and voltage losses due to irreversibility:

$$E_{\text{cell}} = E_{\text{rev}} - \eta_N - \eta_O - \eta_{\text{act}} - \eta_{\text{conc}}, \tag{18}$$

**Fig. 3** Boundary conditions for the heat exchanger methane/steam reformer model

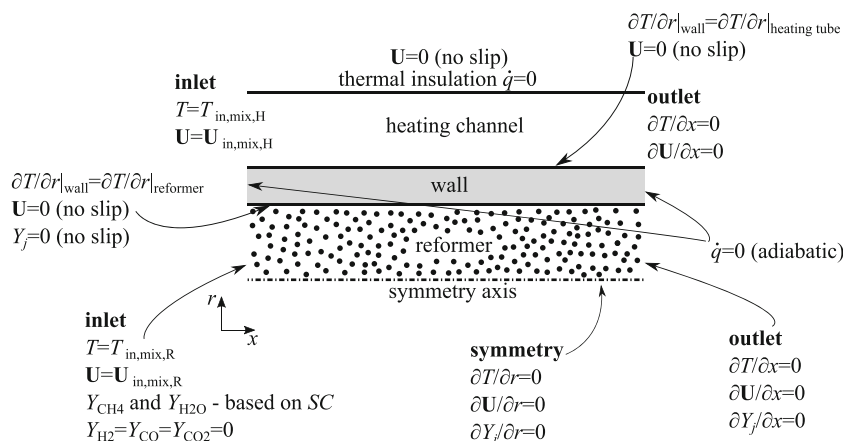




**Table 2** Physical parameters for the model [7]

$R_{\text{cell}}$ [ $\Omega \text{ m}^2$ ]	$i_0$ [ $\text{A m}^{-2}$ ]
$-7.54 \cdot 10^{-8} T + 6.659 \cdot 10^{-5}$	$4.98 T - 2603$

where  $\eta$  terms are overpotentials, which are responsible for voltage losses.

The Nernst term,  $\eta_N$  can describe potential losses due to the concentration of species in the cell:

$$\eta_N = \frac{\bar{R}T}{2F} \ln \left( \frac{p_{\text{H}_2\text{O}}}{p_{\text{H}_2} p_{\text{O}_2}^{0.5}} \right). \quad (19)$$

It should be noted that open circuit voltage, the voltage commonly used in fuel cell analysis, depends on the Nernst term due to the well-known Nernst equation [12]:

$$OCV = E_{\text{rev}} - \eta_N. \quad (20)$$

Ohmic polarization is a result of a current flow, primarily through the electrolyte and may be derived from Ohm's law as [7]:

$$\eta_O = i \cdot R_{\text{cell}}, \quad (21)$$

where  $R_{\text{cell}}$  is the electrolyte area-specific resistance (see Table 2).

Activation polarization is described by the Tafel equation assuming that the load is always higher than the exchange current density  $i_0$ .

$$\eta_{\text{act}} = c + e \ln i. \quad (22)$$

Anode activation polarization is small in comparison with cathode activation polarization, thus in the current model it is neglected [7]. The parameters of the Tafel equation are  $c = -(\bar{R}T)/(2F) \ln i_0$  and  $e = (\bar{R}T)/(2F)$ . The cathodic exchange current density  $i_0$  is presented in Table 2. To achieve the correctness of the Tafel equation, the actual load should not be less than  $0.2 \text{ A cm}^{-2}$ .

Concentration polarization depends on the gas transport into the porous electrodes and it is different for the anode and cathode. For the anode:

$$\eta_{\text{conc}}^{\text{anode}} = \frac{\bar{R}T}{2F} \ln \left( 1 + \frac{p_{\text{H}_2}}{p_{\text{H}_2\text{O}}} \frac{i}{i_{\text{lim}}^{\text{anode}}} \right) - \frac{\bar{R}T}{2F} \ln \left( 1 - \frac{i}{i_{\text{lim}}^{\text{anode}}} \right), \quad (23)$$

and for the cathode:

$$\eta_{\text{conc}}^{\text{cathode}} = -\frac{\bar{R}T}{4F} \ln \left( 1 - \frac{i}{i_{\text{lim}}^{\text{cathode}}} \right), \quad (24)$$

where  $i_{\text{lim}}$  are the limiting current densities, which is the maximal possible current density produced in the half cell reaction.

$$i_{\text{lim}}^{\text{anode}} = \frac{2F p_{\text{H}_2} \bar{D}_{\text{eff}}}{\bar{R}T d_{\text{anode}}}, \quad (25)$$

$$i_{\text{lim}}^{\text{cathode}} = \frac{4F p_{\text{O}_2} \bar{D}_{\text{eff}}}{\bar{R}T d_{\text{cathode}}} \frac{P - p_{\text{O}_2}}{P}, \quad (26)$$

where  $\bar{D}$  is the average diffusion coefficient in [ $\text{m}^2 \text{ s}^{-1}$ ] and  $d$  stands for the electrode thickness. Diffusion coefficients were calculated using the Fuller et al. method [20] and they take into account the binary diffusion, the Knudsen diffusion as well as the effect of the electrode porosity and tortuosity.

The power of the cell may be calculated as a product of current and potential:

$$P_{\text{cell}} = E_{\text{cell}} i A_{\text{cell}}, \quad (27)$$

where  $A_{\text{cell}}$  is the cell area. The cell efficiency is given by [12]:

$$\varepsilon_{\text{cell}} = \frac{E_{\text{cell}}}{E_{\text{tn}}} U_f, \quad (28)$$

where  $E_{\text{tn}} = -\Delta h / 2F$  is the thermoneutral voltage, i.e. the voltage achieved, if the chemical energy which had been provided with the fuel and oxidant would have gotten completely converted into electricity. One should note that the thermoneutral voltage calculation is conducted on the lower heating value basis.  $U_f$  is the utilization factor and  $0 \leq U_f \leq 1$ . For the SOFCs, it is common that the utilization factor is about 0.7-0.8 to keep the safe operation conditions. Utilization is calculated according to Komatsu et al. [11]:

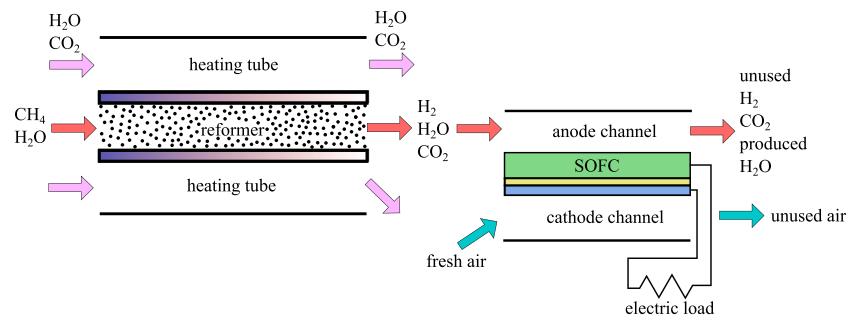
$$U_f = \frac{i A_{\text{cell}}}{2F \dot{n}_{\text{H}_2}^{\text{inlet}}}. \quad (29)$$

To achieve that fuel utilization factor  $U_f$  will be always kept between the limits, maximum possible current density is calculated for  $U_f = 1$ :

$$i_{\text{max}} = \frac{2F \dot{n}_{\text{H}_2}^{\text{inlet}}}{A_{\text{cell}}}. \quad (30)$$

**Table 3** Solid oxide fuel cell design [5, 8]

	Porosity $\varphi$ [-]	Tortuosity $\tau$ [-]	Thickness $d$ [ $\mu\text{m}$ ]	Cell area $A_{\text{cell}}$ [ $\text{m}^2$ ]
Anode	0.49	1.74	240	50
Cathode	0.26	2.63	50	

**Fig. 4** Scheme of connection between reformer and SOFC

Several of the parameters for the foregoing equations are derived from the measurements. The linear functions presented in Table 2 are approximations due to the data of Kim et al. [7]; these relations are valid in the temperature range 650–800 °C. The design of the SOFC which is taken into consideration in this study is described in Table 3. The anode and cathode pore microstructure parameters are taken from the works of Kishimoto [8] and Gostovic [5], respectively.

Both of the models presented above are conjugated (see Fig. 4). The gas composition at the reformer outlet is the same as the composition at the cell inlet. Moreover, the mass flux at the reformer inlet equals the mass flux at the cell outlet.

### 3 Results

The numerical computations to investigate the performance of the heat exchanger-type methane steam reformer have been conducted. The boundary conditions are presented in Table 4 (in Table 4 the label ‘reformer’ means that gases instantly approach reformer temperature, i.e.  $\partial T/\partial x = 0$  at the reactor inlet); case 1 is treated as a reference case. Only the differences between the cases are shown in Table 4; other parameters are treated as the same for every set of computations and they are set as follows:

- the heating channel inlet composition 30% CO<sub>2</sub>+ 70% H<sub>2</sub>O,
- the heating channel inlet temperature  $T_{\text{mix,H}}^{\text{in}} = 1300$  K,
- the catalyst weight density  $w_{\text{cat}} = 1 \cdot 10^3$  kg m<sup>-3</sup>.

The results from the computations have been utilized in the SOFC model to predict the current-voltage and current-power characteristics as well as to check the cell efficiency.

#### 3.1 Heat exchanger-type methane steam reformer

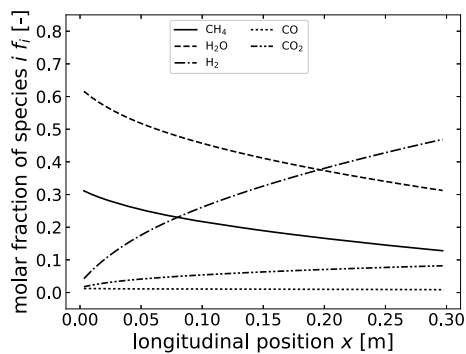
The results of the numerical computations for the heat exchanger-type methane/steam reformer are presented in Figs. 5, 6, 7 and 8. The boundary conditions for every case are presented in Table 4.

It can be seen that the methane conversion rate is strongly influenced by the amount of enthalpy provided at the system inlet. For cases 1 and 2 (see Figs. 5b and 6b), the energy carried by the mixture of CO<sub>2</sub> and H<sub>2</sub>O is the same, however, the enthalpy of the fuel is higher in case 2 seeing that the fuel inlet temperature is substantial (900 K). The amount of energy provided by the fuel is sufficient to activate the methane/steam reforming reaction instantly when the gases contact the catalyst, whereas in the reference case, thermal energy is necessary to heat up the gases, which results in slow methane conversion in the inlet part of the reactor (Fig. 5a). However, the temperature profile inside the heating channel is almost unaffected with this phenomena, because of the low thermal conductivity of the separating wall, which leads to the conclusion that heat conductivity of the wall material should be as high as possible. Notwithstanding, the heating tube it is necessary to keep the wall temperature at the high level.

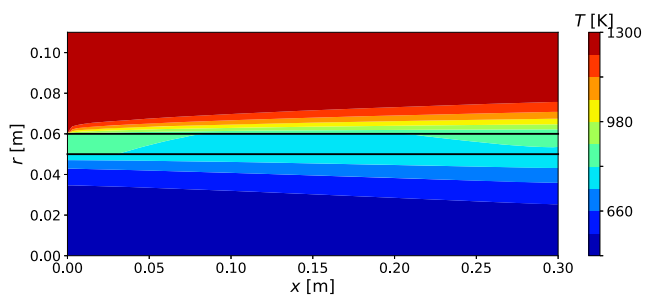
A noticeable drop in the heating channel temperature occurs when the velocities of the CO<sub>2</sub>/H<sub>2</sub>O mixture and fuel mixture are lower, as shown in Figure 7b. It is induced by a considerable gas hourly space velocity (GHSV); this

**Table 4** Boundary conditions for reforming unit model

	Case 1	Case 2	Case 3	Case 4
The reformer inlet temperature $T_{\text{mix,R}}^{\text{in}}$ [K]	Reformer	900	Reformer	Reformer
The reformer inlet velocity $u_{\text{mix,R}}^{\text{in}}$ [m s <sup>-1</sup> ]	0.25	0.25	0.1	0.25
The heating channel inlet velocity $u_{\text{mix,H}}^{\text{in}}$ [m s <sup>-1</sup> ]	1.0	1.0	0.25	1.0
The steam-to-methane ratio at the reformer inlet $SC$ [–]	2.0	2.0	2.0	4.0

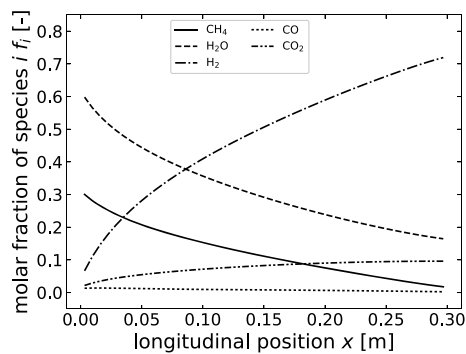


(a) Averaged molar fractions along the reformer

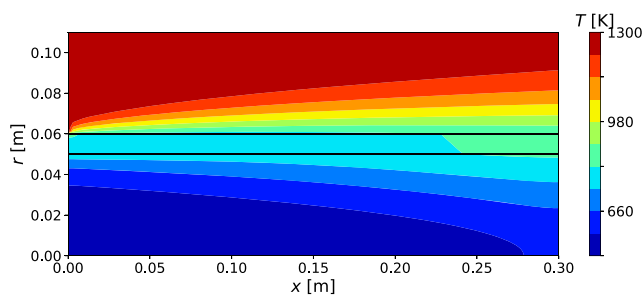


(b) Temperature field inside the reforming unit

Fig. 5 Results of the computations: case 1 (reference)

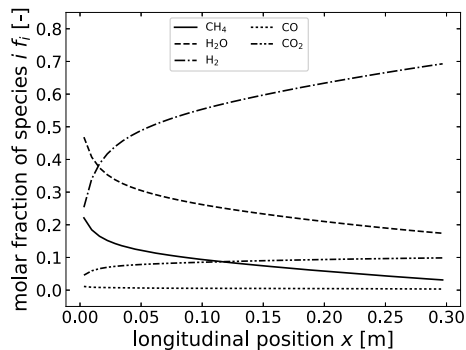


(a) Averaged molar fractions along the reformer

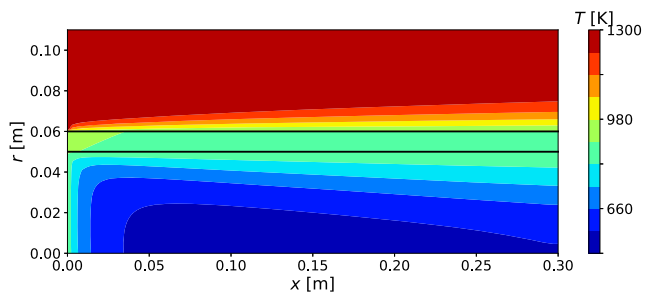


(b) Temperature field inside the reforming unit

Fig. 7 Results of the computations: case 3

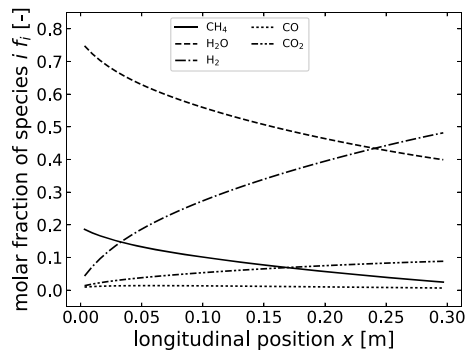


(a) Averaged molar fractions along the reformer

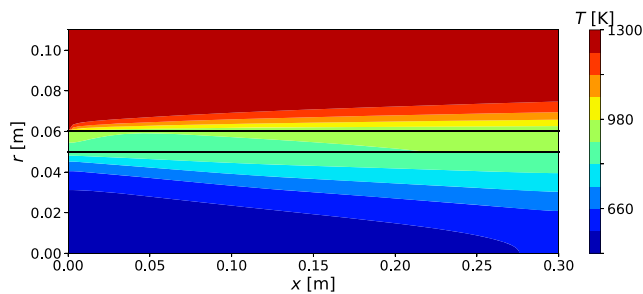


(b) Temperature field inside the reforming unit

Fig. 6 Results of the computations: case 2



(a) Averaged molar fractions along the reformer



(b) Temperature field inside the reforming unit

Fig. 8 Results of the computations: case 4



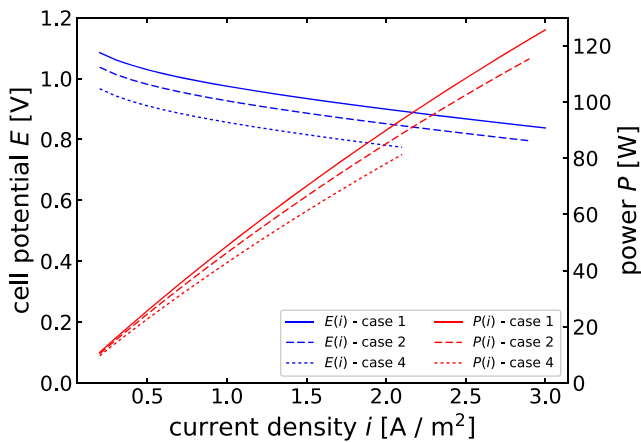


**Fig. 9** Current-voltage and current-power characteristics of the SOFC fueled with the reformed methane

parameter describes how long fuel stays inside the reactor. When the GHSV is low (which means that the fuel velocity is low), the heat is transferred more efficiently, even though the wall is characterized by low thermal conductivity. In this case, the amount of produced hydrogen is the highest among the results presented in this paper and there is almost no methane at the reactor outlet (see Fig. 7a).

Increasing the steam-to-methane ratio ( $SC$ ) from 2.0 to 4.0 does not affect the temperature field strongly (compare Figs. 5b and 8b). However, the methane conversion rate is higher than in the reference case (see Figs. 5a and 8a), which indicates that in case 1 ( $SC = 2.0$ ) the reforming reactor is too short, because the methane conversion should be around 100% for a well-designed reactor. Moreover, the amount of produced hydrogen is the same for both cases. These phenomena are caused by a lower molar fraction of methane at the reactor inlet. Due to a higher molar fraction of water at the reformer outlet, the change of  $SC$  ratio may affect the efficiency of the SOFC fueled by the gases from the methane/steam reformer, by Eqs. 19 and 20.

### 3.2 Solid oxide fuel cell

The outlet composition from Section 3.1 is treated as an input composition for the SOFC power and efficiency calculations. The results from cases 1, 2 and 4 (see Table 4) have been utilized in the SOFC characteristics and efficiency calculation. It is assumed that the unreacted carbon monoxide and methane reacts with the steam on the nickel anode, which serves as a catalyst; this assumption is justified because the kinetics of water-gas shift and methane/steam reforming are faster than the kinetics of the

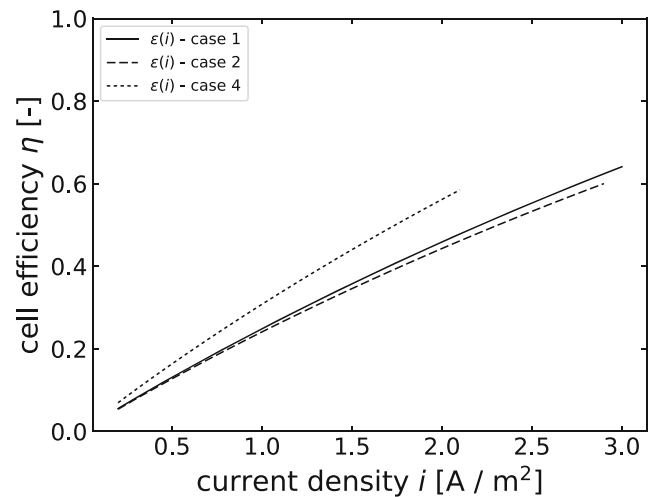


**Fig. 10** Efficiency of the SOFC fueled with the reformed methane

electrochemical oxidation of CO and CH<sub>4</sub>. Cell working temperature was set as 1100 K and the device operates under atmospheric pressure.

The results are presented on Figs. 9 and 10. The fuel composition before and after direct reforming on anode is presented in Table 5.

The larger the molar fraction of the hydrogen is in the fuel, the higher is the maximal current density. This effect is connected with later attendance of the utilization factor (see Fig. 9). This is the reason why the maximum power is achieved for the case with the highest amount of hydrogen in the fuel after direct reforming, which is case 1. As can be seen in Fig. 9, the lowest power and cell potential for a given current density are reached by the SOFC fueled with the fuel mixture from case 4, i.e. when the  $SC$  ratio was high. This phenomenon is caused by the high amount of water vapor, which below some amount has a negative effect on the OCV (see Eqs. 19 and 20).

However, the authors' analysis of SOFC efficiency presented in Fig. 10, shows that for a given current density energy is converted more efficiently for the cell operating on fuel from the case 4. The relatively low cell potential and maximum current density achieved for this fuel may be overcome when the SOFCs are connected in a stack. It is worth to note, that for a given temperature and mass flow rate maximum efficiency is similar for every case. For the highest possible current density, the efficiency achieved from the fuel produced in the reformer operating due to the parameters labeled as case 1, is several percent higher than in case 2 and 3, but it is dangerous for the fuel cells to operate at such high fuel utilization factors.

**Table 5** Molar fractions of the fuel components

	Before direct reforming			After direct reforming		
	Case 1	Case 2	Case 4	Case 1	Case 2	Case 4
H <sub>2</sub>	0.47	0.69	0.48	0.79	0.77	0.56
H <sub>2</sub> O	0.31	0.17	0.40	0.04	0.10	0.33
CO	0.01	0.01	0.01	0.00	0.00	0.00
CO <sub>2</sub>	0.08	0.10	0.09	0.17	0.13	0.11
CH <sub>4</sub>	0.13	0.03	0.02	0.00	0.00	0.00

## 4 General conclusions

The analysis of a methane/steam reformer heated by a hot gas mixture which is produced from the combustion of the remains of fuel from a solid oxide fuel cell has been carried out. It is proven that SOFC can thermally support a hydrogen production system if the heat exchanger-type methane/steam reforming reactor is adopted. It is also possible to achieve a high methane conversion rate.

Moreover, the zero-dimensional model of SOFC has been formulated, and it is shown that the syngas produced during the reforming process may be utilized in a solid oxide fuel cell. This is one of the possible applications for an afterburner-heated reformer. In the above-mentioned case, the high *SC* ratio, which for the methane/steam reforming is not always desirable, has a positive effect on cell efficiency. The problem with relatively poor cell characteristics (potential and power), which arise in the discussed case, can be bypassed by connecting SOFCs in stacks.

**Acknowledgements** The presented work was supported by the FIRST TEAM programme (grant no. First TEAM/2016-1/3) of the Foundation for Polish Science co-financed by the European Union under the European Regional Development Fund. The numerical computations made use of computational resources provided by the PL-Grid (Prometheus computing cluster).

## Compliance with Ethical Standards

**Conflict of interest statement** On behalf of all authors, the corresponding author states that there is no conflict of interest.

**Open Access** This article is distributed under the terms of the Creative Commons Attribution 4.0 International License (<http://creativecommons.org/licenses/by/4.0/>), which permits unrestricted use, distribution, and reproduction in any medium, provided you give appropriate credit to the original author(s) and the source, provide a link to the Creative Commons license, and indicate if changes were made.

## Publisher's Note

Springer Nature remains neutral with regard to jurisdictional claims in published maps and institutional affiliations.

## References

- Ahmed K, Föger K (2001) Approach to equilibrium of the water-gas shift reaction on a Ni/zirconia anode under solid oxide fuel-cell conditions. *J Power Sources* 103(1):150–153
- Brus G, Szmyd JS (2008) Numerical modelling of radiative heat transfer in an internal indirect reforming-type SOFC. *J Power Sources* 181(1):8–16
- Brus G, Kimijima S, Szmyd JS (2012) Experimental and numerical analysis of transport phenomena in an internal indirect fuel reforming type Solid Oxide Fuel Cells using ni/SDC as a catalyst. *J Phys Conf Ser* 395:012,159
- Brus G, Miyoshi K, Iwai H, Saito M, Yoshida H (2015) Change of an anode's microstructure morphology during the fuel starvation of an anode-supported solid oxide fuel cell. *Int J Hydrog Energy* 40(21):6927–6934
- Gostovic D, Smith JR, Kundinger DP, Jones KS, Wachsmann ED (2007) Three-Dimensional Reconstruction of porous LSCF cathodes. *Electrochem Solid-State Lett* 10(12):B214–B217
- Iwai H, Yamamoto Y, Saito M, Yoshida H (2011) Numerical simulation of intermediate-temperature direct-internal-reforming planar solid oxide fuel cell. *Energy* 36(4):2225–2234
- Kim JW, Virkar AV, Fung KZ, Mehta K, Singhal SC (1999) Polarization effects in intermediate temperature, Anode-Supported solid oxide fuel cells. *J Electrochem Soc* 146(1):69–78
- Kishimoto M, Iwai H, Saito M, Yoshida H (2011) Quantitative evaluation of solid oxide fuel cell porous anode microstructure based on focused ion beam and scanning electron microscope technique and prediction of anode overpotentials. *J Power Sources* 196(10):4555–4563
- Klein JM, Bultel Y, Georges S, Pons M (2007) Modeling of a SOFC fuelled by methane: From direct internal reforming to gradual internal reforming. *Chem Eng Sci* 62(6):1636–1649
- Komatsu Y, Kimijima S, Szmyd JS (2010) Performance analysis for the part-load operation of a solid oxide fuel cell-micro gas turbine hybrid system. *Energy* 35(2):982–988
- Komatsu Y, Brus G, Kimijima S, Szmyd JS (2014) The effect of overpotentials on the transient response of the 300W SOFC cell stack voltage. *Appl Energy* 115:352–359

12. Li X (2005) Principles of fuel cells. Taylor & Francis, New York
13. Mozdierz M, Brus G, Sciazko A, Komatsu Y, Kimijima S, Szmyd JS (2014) An attempt to minimize the temperature gradient along a plug-flow methane/steam reforming reactor by adopting locally controlled heating zones. *J Phys Conf Ser* 530: 012,040
14. Mozdierz M, Brus G, Kimijima S, Szmyd JS (2016) Numerical analysis of helium-heated methane/steam reformer. *J Phys Conf Ser* 745:032,081
15. Mozdierz M, Brus G, Sciazko A, Komatsu Y, Kimijima S, Szmyd JS (2016) Towards a thermal optimization of a Methane/Steam reforming reactor. *Flow Turbul Combust* 97(1):1–19
16. Ni M (2013) 2D heat and mass transfer modeling of methane steam reforming for hydrogen production in a compact reformer. *Energy Convers Manag* 65:155–163
17. Nield DA, Bejan A (2006) Convection in porous media, 3rd edn. Springer Science+Business Media, Inc., New York
18. Nishino T, Szmyd J (2010) Numerical analysis of a cell-based indirect internal reforming tubular sofc operating with biogas. *J Fuel Cell Sci Technol* 7:1–8
19. Nishino T, Iwai H, Suzuki K (2006) Comprehensive numerical modeling and analysis of a cell-based indirect internal reforming tubular SOFC. *ASME Journal of Fuel Cell Science and Technology* 3(1):33–44
20. Poling BE, Prausnitz JM, O'Connell JP (2001) The properties of gases and liquids, 5th edn. McGraw-Hill, New York
21. Powell M, Meinhardt K, Sprenkle V, Chick L, McVay G (2012) Demonstration of a highly efficient solid oxide fuel cell power system using adiabatic steam reforming and anode gas recirculation. *J Power Sources* 205:377–384
22. Sciazko A, Komatsu Y, Brus G, Kimijima S, Szmyd JS (2014) A novel approach to improve the mathematical modelling of the internal reforming process for solid oxide fuel cells using the orthogonal least squares method. *Int J Hydrog Energy* 39(29): 16,372–16,389
23. Sciazko A, Komatsu Y, Brus G, Kimijima S, Szmyd JS (2014) A novel approach to the experimental study on methane/steam reforming kinetics using the Orthogonal Least Squares method. *J Power Sources* 262:245–254
24. Song TW, Sohn JL, Kim JH, Kim TS, Ro ST, Suzuki K (2005) Performance analysis of a tubular solid oxide fuel cell/micro gas turbine hybrid power system based on a quasi-two dimensional model. *J Power Sources* 142(1-2):30–42
25. Sucipta M, Kimijima S, Suzuki K (2007) Performance analysis of the SOFC-MGT hybrid system with gasified biomass fuel. *J Power Sources* 174:124–135
26. Todd B, Young J (2002) Thermodynamic and transport properties of gases for use in solid oxide fuel cell modelling. *J Power Sources* 110(1):186–200
27. Xu J, Froment GF (1989) Methane steam reforming, methanation and Water-Gas shift: i. Intrinsic kinetics. *AIChE J* 35(1):88–96
28. Yin H, Jiang S, Zhang Y, Ju H (2007) Modeling of the Helium-Heated steam reformer for HTR-10. *J Nucl Sci Technol* 44(7):977–984
29. Zhu H, Kee RJ (2006) Thermodynamics of SOFC efficiency and fuel utilization as functions of fuel mixtures and operating conditions. *J Power Sources* 161(2):957–964